Universität des Saarlandes

Fachrichtung 6.1 – Mathematik

Preprint Nr. 357

Convection-adapted BEM-based FEM

Clemens Hofreither, Ulrich Langer and Steffen Weißer

Saarbrücken 2015

Fachrichtung 6.1 – Mathematik
Universität des Saarlandes

Preprint No. 357
submitted: 20.02.2015

Convection-adapted BEM-based FEM

Clemens Hofreither
Johannes Kepler University Linz
Institute for Computational Mathematics
Altenberger Strasse 69
4040 Linz
Austria
chofreither@numa.uni-linz.ac.at

Ulrich Langer
Austrian Academy of Sciences
Johann Radon Institute for Computational and Applied Mathematics
Altenberger Strasse 69
4040 Linz
Austria
ulrich.langer@ricam.oeaw.ac.at

Steffen Weißer
Saarland University
Department of Mathematics
P.O. Box 15 11 50
66041 Saarbrücken
Germany
weisser@num.uni-sb.de

Edited by
FR 6.1 – Mathematik
Universität des Saarlandes
Postfach 15 11 50
66041 Saarbrücken
Germany

Fax: + 49 681 302 4443
e-Mail: preprint@math.uni-sb.de
WWW: http://www.math.uni-sb.de/

Convection-adapted BEM-based FEM

Clemens Hofreither Ulrich Langer Steffen Weißer

February 20, 2015

Abstract

We present a new discretization method for homogeneous convection-diffusion-reaction boundary value problems in 3D that is a non-standard finite element method with PDE-harmonic shape functions on polyhedral elements. The element stiffness matrices are constructed by means of local boundary element techniques. Our method, which we refer to as a BEM-based FEM, can therefore be considered a local Trefftz method with element-wise (locally) PDE-harmonic shape functions. The Dirichlet boundary data for these shape functions is chosen according to a convection-adapted procedure which solves projections of the PDE onto the edges and faces of the elements. This improves the stability of the discretization method for convection-dominated problems both when compared to a standard FEM and to previous BEM-based FEM approaches, as we demonstrate in several numerical experiments.

Keywords Convection-diffusion-reaction problems · non-standard finite element methods · BEM-based FEM · Local Trefftz methods

Mathematics Subject Classification (2000) 65N30, 65N38

1 Introduction

The BEM-based FEM was introduced in [7] on the basis of ideas borrowed from boundary element domain decomposition methods originally proposed by G. C. Hsiao and W. L. Wendland in [19]. This class of discretization methods uses PDE-harmonic shape functions in every element of a polyhedral mesh. In order to generate the local stiffness matrices efficiently, boundary element techniques are employed locally. This is the reason why these non-standard Finite Element Methods are called BEM-based FEM. A BEM-based FEM can also be considered a local Trefftz FEM. The papers [15] and [13] provide the a priori discretization error analysis with respect to the energy and L_2 norms, respectively, where homogeneous diffusion problems serve as model problems. In [25], a new construction of the approximation space was proposed, which employs the polygonal faces of the polyhedral elements. Residual-type a posteriori discretization error estimates were derived in [31] and extended in [36]. These a posteriori discretization error estimates can be used to derive adaptive versions of the BEM-based FEM, see also the PhD thesis by S. Weißer [32]. In addition to the low order approximation techniques, high order trial functions were introduced, discussed and studied in [24, 33, 35], which open the development

towards fully *hp*-adaptive strategies. Fast FETI-type solvers for solving the large linear systems arising from the BEM-based FEM discretization of diffusion problems were studied in [17]. Furthermore, the ideas of the BEM-based FEM are transferred into other application areas. There are, for example, first results on vector valued, $H(\mathrm{div})$-conforming approximations [9] and on time dependent problems [34].
The use of PDE-harmonic shape functions seems to be especially appropriate for convection-diffusion problems. The first results in this direction were presented in [16], see also the PhD thesis by C. Hofreither [14]. The shape functions used in these works are PDE-harmonic in the interior of the polyhedral elements, but their traces on the boundaries of the polyhedral elements are still piecewise linear and not adapted to the convection. There is a close relation between this BEM-based FEM with piecewise linear boundary data and the so-called method of residual-free bubbles [2, 3, 5, 10, 4]. Indeed, it has been shown in [14] that the BEM-based FEM, with exact evaluation of the Steklov-Poincaré operator, is equivalent to the method of residual-free bubbles with exactly computed bubbles. Since the latter has been shown to be a stable method for convection-dominated problems, it seems clear that also the BEM-based FEM should have advantageous stability properties. It should be noted that neither the Steklov-Poincaré operator nor the computation of the residual-free bubbles can be realized exactly in practice. However, the early numerical experiments in [16, 14] demonstrate the stabilizing properties of the BEM-based FEM.
In this paper, we aim to further enhance this stabilizing effect. Our approach is to construct a new BEM-based FEM for convection-diffusion-reaction boundary value problems which employs basis functions that are still PDE-harmonic within the elements, and at the same time convection-adapted on the element boundaries. This adaption to the convection is obtained by solving projected 1D and 2D boundary value problems at all edges and faces of the polyhedral elements, respectively. The projected 1D convection-diffusion-reaction problems on the edges can be solved analytically, whereas the 2D face problems are solved numerically by means of a Streamline Upwind/Petrov-Galerkin (SUPG) finite element method on an auxiliary face triangulation. This approach extends the stable applicability of the new method considerably, as is shown by our numerical experiments.
The remainder of this paper is structured as follows. In Section 2, we derive the skeletal variational formulation that will be the starting point for the discretization. Section 3 provides the boundary integral representations of local Steklov-Poincaré operators. The main results are contained in Section 4, where we construct the convection-adapted PDE-harmonic shape functions and derive a fully discretized skeletal variational formulation as linear systems of algebraic equations. In Section 5, we present and discuss some numerical results illustrating that the convection-adapted BEM-based FEM works well in the convection-dominated case. Finally, Section 6 draws some conclusions and provides an outlook on further work.

2 Derivation

In this section, we briefly derive a so-called skeletal variational formulation for a convection-diffusion-reaction problem. As our model problem, we consider the pure

Dirichlet boundary value problem

$$\begin{aligned} Lu = -\operatorname{div}(A\nabla u) + b\cdot\nabla u + cu = 0 \quad &\text{in } \Omega, \\ u = g \quad &\text{on } \partial\Omega \end{aligned} \tag{1}$$

in a bounded Lipschitz domain $\Omega \subset \mathbb{R}^3$. Here $A(x) \in \mathbb{R}^{3\times 3}$, $b(x) \in \mathbb{R}^3$, and $c(x) \in \mathbb{R}$ are the coefficient functions of the partial differential operator L, and $g \in H^{1/2}(\partial\Omega)$ is the given Dirichlet data. We assume that $A(\cdot)$ is symmetric and uniformly positive, and that $c(\cdot)$ is non-negative. The corresponding variational formulation reads as follows: find $u \in H^1(\Omega)$ with $\gamma_\Omega^0 u = g$ such that

$$\int_\Omega (A\nabla u\cdot\nabla v + b\cdot\nabla u\, v + cuv)\, dx = 0 \qquad \forall\, v \in H_0^1(\Omega), \tag{2}$$

where $\gamma_\Omega^0 : H^1(\Omega) \to H^{1/2}(\partial\Omega)$ refers to the Dirichlet trace operator from the domain Ω to its boundary, and $H_0^1(\Omega) = \{v \in H^1(\Omega) : \gamma_\Omega^0 v = 0\}$. We require that the coefficients A, b, c are $L^\infty(\Omega)$ and that there exists a unique solution of (2).
We assume that we have a finite decomposition $\mathcal{T}$ of Ω into mutually disjoint Lipschitz polyhedra. These will play the role of elements as in a finite element method, but we do not require the existence of a reference element to which the elements can be mapped and instead allow $\mathcal{T}$ to contain an arbitrary mixture of polyhedral element shapes. We require that the coefficients $A(\cdot)$, $b(\cdot)$, and $c(\cdot)$ are piecewise constant with respect to the polyhedral mesh $\mathcal{T}$.
It follows from the variational formulation and the density of $C_0^\infty(T)$ in $L_2(T)$ that $\operatorname{div}(A\nabla u) = b\cdot\nabla u + cu \in L_2(T)$ for every element $T \in \mathcal{T}$. Therefore, the flux $A\nabla u$ is in $H(\operatorname{div}, T)$. Let n_T denote the outward unit normal vector on ∂T. Then the flux has a well-defined normal trace $\gamma_T^1 u = A\nabla u\cdot n_T \in H^{-1/2}(\partial T)$, also called the *conormal derivative* of u (cf. [11]). Moreover, we have the generalized Green's identity

$$\int_T A\nabla u\cdot\nabla v\, dx = -\int_T \operatorname{div}(A\nabla u) v\, dx + \langle \gamma_T^1 u,\, \gamma_T^0 v\rangle \qquad \forall v \in H^1(T), \tag{3}$$

where $\langle\cdot,\cdot\rangle$ denotes the duality pairing on $H^{-1/2}(\partial T)\times H^{1/2}(\partial T)$. We mention that the particular element boundary ∂T will always be clear by context. Inserting (3) into (2) and recalling that $Lu = 0$ in $L_2(T)$, we obtain

$$0 = \sum_{T\in\mathcal{T}} \int_T (A\nabla u\cdot\nabla v + b\cdot\nabla u\, v + cuv)\, dx = \sum_{T\in\mathcal{T}} \Big(\underbrace{\int_T Lu\, v\, dx}_{=0} + \langle \gamma_T^1 u,\, \gamma_T^0 v\rangle \Big).$$

Fix now some element $T \in \mathcal{T}$ and observe that $u|_T$ is the unique solution of the local boundary value problem

$$\text{find } \varphi \in H^1(T): \quad L\varphi = 0, \qquad \gamma_T^0\varphi = \gamma_T^0 u. \tag{4}$$

We require that these local problems have unique solutions too. Denoting by $S_T : H^{1/2}(\partial T) \to H^{-1/2}(\partial T)$ the *Steklov-Poincaré operator* or *Dirichlet-to-Neumann*

map for this local problem, we therefore have $\gamma_T^1 u = S_T \gamma_T^0 u$. Writing $u_{\partial T} = \gamma_T^0 u$ and analogously $v_{\partial T}$ for the traces onto the element boundary, we get

$$\sum_{T \in \mathcal{T}} \langle S_T u_{\partial T},\, v_{\partial T} \rangle = 0 \qquad \forall v \in H_0^1(\Omega).$$

Note that all terms in the last formulation are defined only on the element boundaries ∂T. Let $\Gamma_S = \bigcup_T \partial T$ denote the *skeleton* of the mesh $\mathcal{T}$, and let the skeletal function space $W = H^{1/2}(\Gamma_S)$ consist of the traces of all functions from $H^1(\Omega)$ on Γ_S. Then we are looking for a skeletal function $u \in W$ which satisfies the Dirichlet boundary condition $u|_{\partial\Omega} = g$ and the skeletal variational formulation

$$\sum_{T \in \mathcal{T}} \langle S_T u_{\partial T},\, v_{\partial T} \rangle = 0 \qquad \forall\, v \in W_0 = \{ v \in W : v|_{\partial\Omega} = 0 \}\,. \tag{5}$$

This skeletal variational formulation is equivalent to the standard variational formulation (2) in the sense that the traces $u_{\partial T} \in H^{1/2}(\partial T)$ obtained from (5) match the traces $\gamma_T^0 u$ of the function $u \in H^1(\Omega)$ obtained from (2). Conversely, $u|_T$ can be recovered from $u_{\partial T}$ by solving a local Dirichlet problem of type (4) in T. We will call the solution of this local problem the PDE-harmonic extension of $u_{\partial T}$. We remark that another interpretation of (5) is that of a weak enforcement of the continuity of conormal derivatives on inter-element boundaries.

3 Boundary integral operators

Evaluating the Dirichlet-to-Neumann map S_T used above essentially corresponds to solving a local problem $L\varphi = 0$ on T with the given Dirichlet data and then obtaining the conormal derivative $\gamma_T^1 \varphi$ of its solution. Even these local problems are in general not analytically solvable and require numerical approximation. At the core of our method, we approximate S_T using a boundary element technique obtained by the Galerkin discretization of element-local boundary integral equations. Some standard results on boundary integral equations are outlined in the following. A more detailed treatment of these topics can be found in, e.g., [20, 23, 28, 30].
An important prerequisite for defining the boundary integral operators is the knowledge of a *fundamental solution*. A fundamental solution of the partial differential operator L is a function $G(x, y)$ such that $L_x G(x, y) = \delta(y - x)$, where δ is the Dirac δ-distribution and $x,\, y \in \mathbb{R}^d$. A fundamental solution for L from (1) with constant coefficients A, b, c is given in [28]. In fact, in $\mathbb{R}^3$ and under the assumption $c + \|b\|_{A^{-1}}^2 \geq 0$, we have

$$G(x, y) = \frac{1}{4\pi\sqrt{\det A}} \frac{\exp\left(b^\top A^{-1}(x - y) - \lambda \|x - y\|_{A^{-1}}\right)}{\|x - y\|_{A^{-1}}}\,,$$

where $\|x\|_{A^{-1}} = \sqrt{x^\top A^{-1} x}$ and $\lambda = \sqrt{c + \|b\|_{A^{-1}}^2}$.
For our setting, we more generally assume that the coefficients A, b, c are constant only within each element. This leads to a potentially different fundamental solution in each element T, in the following denoted by $G_T(x, y)$, and allows us to treat PDEs with piecewise constant coefficients.

We now introduce the local boundary integral operators

$$V_T : H^{-1/2}(\partial T) \to H^{1/2}(\partial T), \quad K_T : H^{1/2}(\partial T) \to H^{1/2}(\partial T),$$
$$K_T' : H^{-1/2}(\partial T) \to H^{-1/2}(\partial T), \quad D_T : H^{1/2}(\partial T) \to H^{-1/2}(\partial T),$$

called, in turn, the *single layer potential*, *double layer potential*, *adjoint double layer potential*, and *hypersingular* operators. For sufficiently regular arguments, they admit the integral representations

$$\begin{aligned}
(V_T v)(y) &= \int_{\partial T} G_T(x,y) v(x)\, ds_x, \\
(K_T u)(y) &= \int_{\partial T} \widetilde{\gamma^1_{T,x}} G_T(x,y) u(x)\, ds_x, \\
(K_T' v)(y) &= \int_{\partial T} \gamma^1_{T,y} G_T(x,y) v(x)\, ds_x, \\
(D_T u)(y) &= -\gamma^1_{T,y} \int_{\partial T} \widetilde{\gamma^1_{T,x}} G_T(x,y) \big(u(x) - u(y)\big)\, ds_x,
\end{aligned}$$

where $\gamma^1_{T,y}$ refers to the conormal derivative γ^1_T with respect to the variable y, whereas $\widetilde{\gamma^1_{T,x}}$ refers to the modified conormal derivative with respect to x, i.e.,

$$\widetilde{\gamma^1_T} u = \gamma^1_T u + (b \cdot n_T)\gamma^0_T u,$$

which is associated with the adjoint problem. We have the following two representations of the Steklov-Poincaré operator in terms of the boundary integral operators:

$$S_T = V_T^{-1}(\tfrac{1}{2} I + K_T) = D_T + (\tfrac{1}{2} I + K_T') V_T^{-1} (\tfrac{1}{2} I + K_T). \tag{6}$$

4 Discretization

4.1 Discretization of the skeletal function space

We employ a Galerkin approach to the discretization of the skeletal variational formulation (5). To this end, we notice that every element boundary ∂T is composed of open polygonal faces $\mathcal{F}_T$, straight edges $\mathcal{E}_T$ and nodes $\mathcal{N}_T$ located in the corner points of the element. Neighboring elements either share a common face, edge or node. This gives a natural description of the skeleton $\overline{\mathcal{F}} = \bigcup_{T \in \mathcal{T}} \overline{\mathcal{F}}_T$ of the decomposition $\mathcal{T}$. In the following, we construct a discrete trial space $W_h \subset W$ over $\mathcal{F}$. The PDE-harmonic extensions of its basis functions can thus be interpreted as three dimensional trial functions for the approximation of u.
If the skeleton $\mathcal{F}$ consists only of triangular faces or if it is triangulated, a straightforward choice for W_h is the space of piecewise linear and globally continuous functions on $\mathcal{F}$. This strategy was introduced in [16] for the convection-diffusion-reaction equation. An enhanced strategy was proposed in [25] for the pure diffusion equation. It makes use of a hierarchical construction of trial functions on polyhedral

elements with polygonal faces. Extending this idea, we define the basis functions of W_h with the help of PDE-harmonic extensions on edges and faces, which might be triangles or of polygonal shape.
More precisely, for each node $z_i \in \mathcal{N} = \bigcup_{T\in\mathcal{T}} \mathcal{N}_T$, we introduce a skeletal basis function $\varphi_i \in W$ satisfying

$$\begin{aligned} \varphi_i(z_j) &= \delta_{ij} \quad \text{for } z_j \in \mathcal{N}, \\ L_E\varphi_i &= 0 \quad \text{on } E \in \mathcal{E}, \\ L_F\varphi_i &= 0 \quad \text{on } F \in \mathcal{F}, \end{aligned} \tag{7}$$

where L_E and L_F are projections of the differential operator L onto the edge E and face F, respectively, and $\mathcal{E} = \bigcup_{T\in\mathcal{T}} \mathcal{E}_T$. Thus, the functions φ_i are defined implicitly as local solutions of boundary value problems on edges and faces of the decomposition. Equivalently, one can say that these functions are defined via PDE-harmonic extensions. The nodal data is first extended L_E-harmonically along the edges and afterwards, the data on the edges is extended into the faces with the help of a L_F-harmonic operator.
For the definition of L_E and L_F, let $F \in \mathcal{F}$ be a face and $E \in \mathcal{E}$ an edge on the boundary of F. By rotation and translation of the coordinate system, we map the face F into the (e_1, e_2)-plane and the edge E onto the e_1-axis of the Euclidean coordinate system (e_1, e_2, e_3) such that one node of E lies in the origin. Thus, we have an orthogonal matrix $B \in \mathbb{R}^{3\times3}$ and a vector $d \in \mathbb{R}^3$ such that

$$\tilde{x} \mapsto x = B\tilde{x} + d \quad \text{and} \quad \tilde{\varphi}(\tilde{x}) = \varphi(B\tilde{x} + d),$$

and the differential equation in (1) yields

$$-\operatorname{div}(A\nabla\varphi) + b\cdot\nabla\varphi + c\varphi = -\operatorname{div}_{\tilde{x}}(BAB^\top\nabla_{\tilde{x}}\tilde{\varphi}) + Bb\cdot\nabla_{\tilde{x}}\tilde{\varphi} + c\tilde{\varphi} = 0. \tag{8}$$

Furthermore, we assume for the definition of trial functions that they only vary in tangential direction to the face and edge, respectively, i.e., $\frac{\partial\tilde{\varphi}}{\partial\tilde{x}_3} = 0$ in F and $\frac{\partial\tilde{\varphi}}{\partial\tilde{x}_2} = \frac{\partial\tilde{\varphi}}{\partial\tilde{x}_3} = 0$ on E. Therefore, the dependence in (8) reduces to two and one coordinate directions such that L_F and L_E are defined as differential operators in two and one dimensions using the described coordinate system. Overall, the basis functions are constructed with the help of the convection-diffusion-reaction equation on the faces and edges, where the diffusion matrix and the convection vector are adjusted in a proper way.
Attentive readers have noticed that A, b and c are assumed to be constant on each polygonal subdomain such that they are not well-defined on faces and edges. Therefore, in order to make the operators L_E and L_F well-defined, we have to understand A, b and c in (8) on F and E as averaged quantities over the neighboring polyhedra of the face F and the edge E, respectively. To simplify notation, we will omit the coordinate transformation in the following and abbreviate the transformed diffusion matrix $BAB^\top$ and convection vector Bb to A_F and b_F, respectively. Furthermore, we will treat the basis functions φ_i as functions of two or one variable depending on the underlying domain F or E.
Having defined the basis functions φ_i, we obtain a discretization space $W_h = \operatorname{span}\{\varphi_i : i = 1, \dots, |\mathcal{N}|\} \subset W$, where $|\mathcal{N}|$ denotes the number of nodes in the

polyhedral mesh. Assuming that the given Dirichlet data g can be extended to the skeleton by a function in W_h, we thus arrive at the following Galerkin equations as the discrete version of (5): find $u_h \in W_h$ such that $u_h|_{\partial\Omega} = g$ and

$$\sum_{T\in\mathcal{T}} \langle S_T u_{h,\partial T},\, v_{h,\partial T}\rangle = 0 \qquad \forall\, v_h \in W_{h,0} = W_h \cap W_0. \tag{9}$$

In the general case, the Dirichlet data g can be approximated by the introduced trial functions $\varphi \in W_h$ using interpolation (if continuous) or L_2-projection.

4.2 Approximation of the skeletal basis functions

The construction of the skeletal basis functions $\{\varphi_i\}$ involves the solution of certain lower-dimensional boundary value problems which cannot, in general, be done exactly. In this section, we therefore construct computable approximations to the exact basis functions.

In (7), L_E describes an ordinary differential operator of second order with constant and scalar-valued coefficients. Thus the boundary value problems on the edges can be solved analytically and the restrictions of the functions in W_h to each edge $E \in \mathcal{E}$ can be written in closed form.

The two-dimensional problems involving the operator L_F on the faces, however, need to be solved approximately. We choose a SUPG method, see [6], on each face since we might have convection-dominated problems there. To this end, we introduce an auxiliary triangulation of each face in such a way that the meshes are matching on common edges as well as quasi-uniform and shape-regular in the usual sense, with constants which are uniform over all faces $F \in \mathcal{F}$. In the case of elements and faces which are star-shaped with respect to a ball and a circle, respectively, we can use, for example, the construction in [25]. Here, a first coarse triangulation of a face $F \in \mathcal{F}$ is obtained by connecting its nodes with the center of the inscribed circle. This auxiliary mesh is denoted by $\mathfrak{T}_0(F)$. Afterwards, the meshes $\mathfrak{T}_\ell(F)$ of level $\ell \geq 1$ are defined recursively by splitting each triangle of the previous level into four similar triangles by connecting its edge midpoints. This strategy yields a conforming triangulation $\mathfrak{T}_\ell(\mathcal{F}_T) = \bigcup_{F\in\mathcal{F}_T} \mathfrak{T}_\ell(F)$ of the surface of the polyhedral elements, see Figure 1, as well as a conforming triangulation $\mathfrak{T}_\ell(\mathcal{F}) = \bigcup_{F\in\mathcal{F}} \mathfrak{T}_\ell(F)$ of the whole skeleton. Furthermore, it also induces a discretization of each edge $E \in \mathcal{E}$ into line segments of equal size which we denote by $\mathfrak{T}_\ell(E)$.

Let $\mathfrak{W}_\ell(\mathcal{F})$ denote the space of piecewise linear functions over the auxiliary triangulation $\mathfrak{T}_\ell(\mathcal{F})$ which are continuous on the skeleton. We denote the restrictions of $\mathfrak{W}_\ell(\mathcal{F})$ onto a face F and the boundary ∂T of an element by $\mathfrak{W}_\ell(F)$ and $\mathfrak{W}_\ell(\mathcal{F}_T)$, respectively. Furthermore, let $\mathfrak{W}_{\ell,0}(F)$ be the subspace of $\mathfrak{W}_\ell(F)$ which contains only functions vanishing on the boundary of F.

Now, we have the ingredients to handle the approximation of the basis functions on the faces. For any $\varphi_i \in W_h$, we define its approximation $\varphi_\ell^i \in \mathfrak{W}_\ell(F)$ on each face $F \in \mathcal{F}$ with $z_i \in \partial F$ such that it coincides with the piecewise linear (with respect to $\mathfrak{T}_\ell(E)$) nodal interpolation of φ_i on the edges of F and such that it fulfills the SUPG formulation: find $\varphi_\ell^i \in \mathfrak{W}_\ell(F)$ such that boundary conditions on ∂F, as described

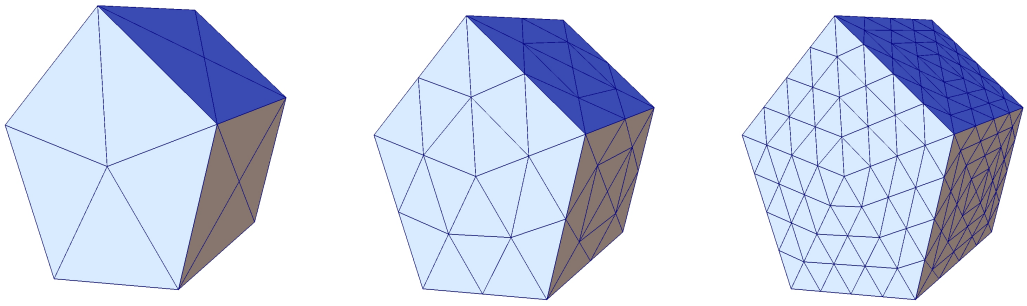

Figure 1: Auxiliary triangulation $\mathfrak{T}_\ell(\mathcal{F}_T)$ with $\ell = 0, 1, 2$ for the surface of $T \in \mathcal{T}$.

above, are fulfilled and

$$\int_F (A_F \nabla \varphi_\ell^i \cdot \nabla \phi + b_F \cdot \nabla \varphi_\ell^i \, \phi + c_F \varphi_\ell^i \, \phi) + \delta_F \int_F (b_F \cdot \nabla \varphi_\ell^i \, b_F \cdot \nabla \phi + c_F \varphi_\ell^i \, b_F \cdot \nabla \phi) = 0 \quad \forall \phi \in \mathfrak{W}_{\ell,0}(F), \quad (10)$$

where $\delta_F \geq 0$ is a stabilization parameter which is set to zero in the diffusion-dominated case. On all faces $F \in \mathcal{F}$ with $z_i \notin \partial F$, it is $\varphi_\ell^i \equiv 0$. Finally, we obtain the approximate trial space as $W_\ell = \operatorname{span}\{\varphi_\ell^i : i = 1, \ldots, |\mathcal{N}|\} \subset \mathfrak{W}_\ell(\mathcal{F}) \subset W$. Assuming that the given Dirichlet data g can be extended to the skeleton by a function in W_ℓ, we thus arrive at the following Galerkin equations as the approximated version of (9): find $u_\ell \in W_\ell$ such that $u_\ell|_{\partial\Omega} = g$ and

$$\sum_{T \in \mathcal{T}} \langle S_T u_{\ell,\partial T}, \, v_{\ell,\partial T} \rangle = 0 \qquad \forall \, v_\ell \in W_{\ell,0} = W_\ell \cap W_0. \quad (11)$$

In the general case, the Dirichlet data g can be approximated by the introduced trial functions $\varphi_\ell^i \in W_\ell$ on the boundary faces $F \subset \partial\Omega$ using interpolation (if continuous) or L_2-projection.

4.3 Discretization of the Dirichlet-to-Neumann map

The Dirichlet-to-Neumann maps S_T in (11) will be evaluated via the boundary integral operator representation (6). In the case of diffusion-reaction problems the symmetric representation is preferred, since it preserves the symmetry. In this paper, however, we use the first representation since we deal with a non-symmetric problem. Furthermore, this representation is easier and can be implemented more efficiently. This formula still contains the inverse of the single layer potential operator V_T, which is in general not computable exactly. Hence, we also need to approximate the bilinear form $\langle S_T \cdot, \cdot \rangle$. To do this, we employ a mixed continuous piecewise linear/piecewise constant scheme, where Dirichlet data are approximated linearly, while Neumann data are approximated by piecewise constant functions, as described in, e.g., [8, 30, 18].

Let $\phi_{T,i} \in \mathfrak{W}_\ell(\mathcal{F}_T)$ denote the nodal piecewise linear functions restricted to the local mesh $\mathfrak{T}_\ell(\mathcal{F}_T)$, where now i enumerates the vertices of the auxiliary triangulation $\mathfrak{T}_\ell(\mathcal{F}_T)$. Furthermore, introduce a space of piecewise (per triangle of $\mathfrak{T}_\ell(\mathcal{F}_T)$) constant boundary functions spanned by the basis $\{\psi_{T,k}\}$, where k enumerates the triangles $\tau_k \in \mathfrak{T}_\ell(\mathcal{F}_T)$, such that $\psi_{T,k} \equiv 1$ on τ_k and $\psi_{T,k} \equiv 0$ on all other triangles. For any function $u_T \in H^{1/2}(\partial T)$, its corresponding Neumann data can be written, according to (6), as

$$t_T = S_T u_T = V_T^{-1}(\tfrac{1}{2}I + K_T)u_T \in H^{-1/2}(\partial T).$$

For any piecewise linear function $u_{T\ell} \in \mathfrak{W}_\ell(\mathcal{F}_T) = \operatorname{span}\{\phi_{T,i}\}$, we now compute an approximation $t_{T\ell} \approx t_T$ of its Neumann data by the Galerkin projection of the equation $V_T t_T = (\frac{1}{2}I + K_T)u_T$ to the piecewise constant functions. In other words, we seek $t_{T\ell} \in \operatorname{span}\{\psi_{T,k}\}$ such that

$$\langle \psi_{T,k},\, V_T t_{T\ell}\rangle = \langle \psi_{T,k},\, (\tfrac{1}{2}I + K_T)u_{T\ell}\rangle \qquad \forall k = 1, \dots, |\mathfrak{T}_\ell(\mathcal{F}_T)|.$$

This allows us to define the approximate bilinear form

$$\langle S_T u_{T\ell},\, v_{T\ell}\rangle \approx \langle \widetilde{S}_T u_{T\ell},\, v_{T\ell}\rangle := \langle t_{T\ell},\, v_{T\ell}\rangle, \quad \forall u_{T\ell}, v_{T\ell} \in \mathfrak{W}_\ell(\mathcal{F}_T). \tag{12}$$

Let $\underline{V}_T$, $\underline{K}_T$ and $\underline{\widetilde{S}}_T$ denote the matrices which represent the analytic and approximate bilinear forms induced by the corresponding boundary integral operators with respect to the bases $\{\phi_{T,i}\}$ and $\{\psi_{T,k}\}$, i.e.,

$$[\underline{V}_T]_{kl} = \langle \psi_{T,k},\, V_T \psi_{T,l}\rangle, \quad [\underline{K}_T]_{ki} = \langle \psi_{T,k},\, K_T \phi_{T,i}\rangle, \quad [\underline{\widetilde{S}}_T]_{ij} = \langle \widetilde{S}_T \phi_{T,i},\, \phi_{T,j}\rangle,$$

where i, j enumerate the vertices of $\mathfrak{T}_\ell(\mathcal{F}_T)$, and k, l enumerate the triangles of $\mathfrak{T}_\ell(\mathcal{F}_T)$. Furthermore, let $\underline{M}_T$ denote the mass matrix

$$[\underline{M}_T]_{ki} = \langle \psi_{T,k},\, \phi_{T,i}\rangle.$$

Then, the approximate bilinear form $\langle \widetilde{S}_T \cdot,\, \cdot\rangle$ is realized on our discrete spaces over the element boundary ∂T by the matrix

$$\underline{\widetilde{S}}_T = \underline{M}_T^\top \underline{V}_T^{-1}(\tfrac{1}{2}\underline{M}_T + \underline{K}_T) \in \mathbb{R}^{\dim \mathfrak{W}_\ell(\mathcal{F}_T) \times \dim \mathfrak{W}_\ell(\mathcal{F}_T)}.$$

4.4 Fully discretized variational problem

To obtain the fully discretized variational formulation, we replace the bilinear form in (11) by its approximation (12), i.e., we seek $u_\ell \in W_\ell$ such that $u_\ell|_{\partial\Omega} = g$ and

$$\sum_{T \in \mathcal{T}} \langle \widetilde{S}_T u_{\ell,\partial T},\, v_{\ell,\partial T}\rangle = 0 \qquad \forall\, v_\ell \in W_{\ell,0}. \tag{13}$$

For the sake of clarity, we describe in the following how the linear system resulting from this discretization is constructed. For an approximate basis function φ_ℓ^i, consider its restriction $\varphi_{\ell,\partial T}^i \in \mathfrak{W}_\ell(\mathcal{F}_T)$ to the boundary of the element T. We denote the coefficients of this restriction with respect to the local nodal piecewise linear

basis functions on $\mathfrak{T}_\ell(\mathcal{F}_T)$ by $\underline{\varphi}^i_{\ell,\partial T} \in \mathbb{R}^{\dim \mathfrak{W}_\ell(\mathcal{F}_T)}$. (If $z_i \notin \partial T$, we have $\underline{\varphi}^i_{\ell,\partial T} = 0$.) We gather all these column vectors into a matrix $\underline{D}_T \in \mathbb{R}^{\dim \mathfrak{W}_\ell(\mathcal{F}_T)\times|\mathcal{N}|}$. Then, the global stiffness matrix is assembled element-wise as

$$\underline{K} = \sum_{T\in\mathcal{T}} \underline{D}_T^\top \widetilde{\underline{S}}_T \underline{D}_T \in \mathbb{R}^{|\mathcal{N}|\times|\mathcal{N}|}.$$

After eliminating the Dirichlet boundary conditions by means of homogenization in the usual way, we obtain the final linear system. At this point we should emphasize that the local auxiliary triangulations $\mathfrak{T}_\ell(\mathcal{F}_T)$ are used only to compute the element stiffness matrices. The level of refinement ℓ chosen for them has no influence on the size of the global stiffness matrix.

5 Implementation and numerical examples

In this section, we give some implementation details as well as numerical experiments. The computations are done on tetrahedral and polyhedral meshes. For the sake of simplicity, we restrict ourselves to the case of scalar valued diffusion, i.e., $A = \alpha I$ for some $\alpha > 0$, and a vanishing reaction term $c = 0$. Furthermore, the experiments are carried out with constant and continuously varying convection b. The method is studied for the case of decreasing diffusion $\alpha \to 0$. Standard numerical schemes like the finite element method become unstable when applied to this type of convection-dominated problems. Typically, the issue manifests itself in the form of spurious oscillations. The critical quantity here is the mesh Péclet number

$$\mathrm{Pe}_T = \frac{h_T|b_T|}{\alpha_T}, \quad T \in \mathcal{T},$$

which should be bounded by 2 for standard finite element methods. When decreasing the diffusion, the mesh Péclet number increases and we expect oscillations. This is due to the fact that the boundary value problem gets closer to a transport equation and thus, boundary layers appear near the outflow boundary.
In addition to stability, we study the number of GMRES iterations which are used to compute the approximate solution of the resulting system of linear equations.

5.1 Implementation details

5.1.1 Preprocessing

All computations regarding the convection-adapted trial functions can be done in a preprocessing step. In the case of non-constant convection, diffusion and reaction, these terms are first projected into the space of piecewise constant functions over the edges, faces and elements of the mesh. Afterwards, the Dirichlet traces of the trial functions are computed on the edges and faces. Here, an analytic formula is utilized on each edge $E \in \mathcal{E}$, and subsequently, the two-dimensional convection-diffusion-reaction problems are treated separately on each face $F \in \mathcal{F}$ according to the SUPG

formulation (10). The stabilization parameter δ_F is chosen to be piecewise constant over the auxiliary triangulation $\mathfrak{T}_\ell(F)$ on each face $F \in \mathcal{F}$ with

$$\delta_{F,k} = \begin{cases} h_k/2 & \text{for } \mathrm{Pe}_{F,k} > 2, \\ 0 & \text{else,} \end{cases}$$

where k enumerates the triangles of $\mathfrak{T}_\ell(F)$ and the local Péclet number is defined as

$$\mathrm{Pe}_{F,k} = \frac{h_k |b_F|}{\alpha_F}.$$

The auxiliary triangulations $\mathfrak{T}_\ell(F)$ of level $\ell \in \mathbb{N}_0$ are constructed as described in Section 4 and visualized in Figure 1. But, in case of convection-dominated problems on the faces, we decided to move the midpoint of the mesh, created in $\mathfrak{T}_0(F)$, into the direction of the projected convection vector. Consequently, the auxiliary meshes get adapted to the local problems. This adaptation is inspired by Shishkin-meshes [29], see also [21, 22, 26], which are graded in such a way that boundary layers are resolved. The solutions of the resulting systems of linear equations, coming from the SUPG formulation, with non-symmetric, sparse matrices are approximated using the GMRES method, see [27]. As the stopping criterion, we use the reduction of the norm of the initial residual by a factor of 10^{-10}.
Another preprocessing step is the computation of the matrices arising from the local boundary integral formulations. Here, we use the BEM code developed in the PhD thesis by C. Hofreither [14], which is based on a fully numerical integration scheme described in [28]. The inversions of the local single layer potential matrices $\underline{V}_T$ are performed with an efficient LAPACK routine.

5.1.2 Assembly and solution

The assembling of the global stiffness matrix is performed element-wise as described in Section 4.4. The resulting system of linear equations, which is again sparse and non-symmetric, is treated by GMRES. For the global problem, however, we use the reduction of the norm of the initial residual by a factor of 10^{-6} as the stopping criterion. In our numerical experiments, the GMRES iterations are carried out without preconditioning in general. However, we also implemented a simple geometric row scaling (GRS) preconditioner, see [12], i.e., a diagonal preconditioner

$$C^{-1} = \mathrm{diag}(1/\|\underline{K}_j\|_p),$$

where by $\underline{K}_j$ we mean the j-th row of the global stiffness matrix, and we choose the vector norm with $p = 1$.

5.1.3 Improvements

The proposed method is highly parallelizable, especially the preprocessing steps. The two-dimensional convection-diffusion-reaction problems on the faces are independent of each other, and can thus be treated in parallel. Furthermore, the subsequent setup of the boundary integral matrices and of $\widetilde{\underline{S}}_T$ can be parallelized on an

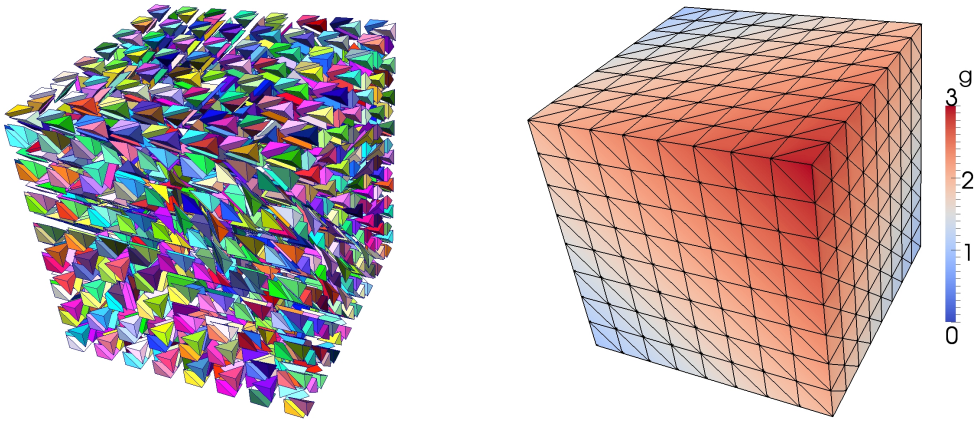

Figure 2: Visualisation of tetrahedral mesh and Dirichlet data for Experiment 1.

element level as well. Even the computations of the single entries of each boundary integral matrix are independent of each other.
In the implementation we use another observation to reduce the computational complexity. In the case of constant convection, diffusion and reaction terms, the local boundary integral matrices and the problems on the edges and faces are identical for elements which differ by some translation only. Therefore, we build a look-up table in a preprocessing step such that redundant computations are avoided.

5.2 Numerical Experiments

5.2.1 Experiment 1

In the first numerical experiment, a problem with constant convection and diffusion terms is studied. Let $\Omega = (0,1)^3$, and let us consider the boundary value problem

$$\begin{aligned} -\alpha\Delta u + b \cdot \nabla u &= 0 \quad \text{in } \Omega, \\ u &= g \quad \text{on } \Gamma, \end{aligned}$$

where $b = (1,0,0)^\top$ and $g(x) = x_1 + x_2 + x_3$. The domain Ω is discretized with tetrahedral elements, see Figure 2. The mesh consists of 3072 elements, 6528 faces, 4184 edges and 729 nodes of which 343 nodes lie in the interior of Ω. Thus, the number of degrees of freedom in the BEM-based FEM is equal to 343 in this example. The maximal element diameter is $h_{\max} \approx 0.22$. The mesh is chosen rather coarse, but it is well suited for the study of stability.
Since the convection and diffusion parameters are constant over the whole domain, the look-up table is applied to speed up the computations. Instead of the before mentioned numbers of geometrical object, we only have to treat 48 elements, 42 faces and 13 edges in the preprocessing step, where the traces of the trial functions are computed and the local stiffness matrices are set up.
To handle the Dirichlet boundary condition, we apply pointwise interpolation of the data g to obtain an extension onto Γ_S. The interpolant is bounded by 0 from below and by 3 from above on Γ. The convection-diffusion problem satisfies the maximum principle and therefore, we know that $0 \leq u \leq 3$ everywhere for the

Table 1: Verifying maximum principle in Experiment 1.

		classic FEM		BEM-based FEM			
		linear		straightforward		hierarchical ($\ell = 2$)	
α	Pe_h	$u_{\min}$	$u_{\max}$	$u_{\min}$	$u_{\max}$	$u_{\min}$	$u_{\max}$
$1.0e-1$	2	0.00	3.00	0.00	3.00	0.00	3.00
$5.0e-2$	4	0.00	3.00	0.00	3.00	0.00	3.00
$2.5e-2$	9	0.00	3.00	0.00	3.00	0.00	3.00
$1.0e-2$	22	−0.55	3.00	0.00	3.00	−0.01	3.00
$5.0e-3$	43	−1.14	3.00	0.00	3.00	−0.01	3.00
$2.5e-3$	87	−1.85	3.07	0.00	3.00	−0.01	3.00
$1.0e-3$	217			0.00	3.00	−0.01	3.00
$5.0e-4$	433			0.00	3.00	−0.01	3.00
$2.5e-4$	866			−142.89	399.06	−0.01	3.00
$1.0e-4$	2165			−68.85	41.00	−0.01	3.00
$5.0e-5$	4330					−0.01	3.08
$2.5e-5$	8660					−0.01	14.72

exact solution. To study stability of the BEM-based FEM, the maximum principle is checked for the approximate solution $u_\ell \in W_\ell$ obtained by (13). Since the trial functions fulfill convection-diffusion problems on the faces and edges and since the maximum principle is also valid there, the maximal values of u_ℓ should by reached in the nodes of the mesh. However, because of oscillations coming from the SUPG methods on the faces, the maximal values might be found at some auxiliary node. Consequently, the maximum principle is tested on the whole skeleton Γ_S.

Table 1 gives a comparison of the classical Finite Element Method with piecewise linear trial functions and without stabilization, the straightforward BEM-based FEM proposed in [16] with linear trial functions on the faces and the new, convection-adapted BEM-based FEM with $\ell = 2$. The classical FEM fulfills the discrete maximum principle until $\alpha = 2.5e-2$, which corresponds to a Péclet number of 9. The BEM-based strategies, which incorporate the behavior of the differential operator into the approximation space, are more stable. The method in [16] passes the test up to $\alpha = 5.0e-4$, which corresponds to $\mathrm{Pe}_h = 433$. In the new, proposed method we might have oscillations occurring in the approximation of the basis functions fulfilling convection-dominated problems on the faces. If we neglect these small deviations in the third digit after the decimal point, the proposed method reaches even $\alpha = 1.0e-4$, i.e. $\mathrm{Pe}_h = 2165$, for $\ell = 2$ without violation of the maximum principle.

Next, we study the influence of the auxiliary triangulations of the faces on the convection-adapted BEM-based FEM. In Table 2, the minimal and maximal values $u_{\min}$ and $u_{\max}$ of the approximate solution are listed for different levels ℓ of the auxiliary meshes. The higher ℓ is chosen, the longer the discrete maximum principle is valid. For $\ell = 3$, we even have stability until $\alpha = 2.5e-5$, i.e., $\mathrm{Pe}_h = 8660$. The enhanced stability can be explained by the improved approximations of the boundary value problems on the edges and faces used to construct the trial functions. Obviously, the local oscillations in the construction of basis functions are reduced such that they have less effect to the global approximation.

Table 2: Verifying maximum principle in Experiment 1 for $\ell = 1, 2, 3$.

		$\ell = 1$		$\ell = 2$		$\ell = 3$	
α	Pe_h	$u_{\min}$	$u_{\max}$	$u_{\min}$	$u_{\max}$	$u_{\min}$	$u_{\max}$
$5.0e-3$	43	-0.01	3.00	-0.01	3.00	0.00	3.00
$2.5e-3$	87	-0.01	3.00	-0.01	3.00	0.00	3.00
$1.0e-3$	217	-0.01	3.00	-0.01	3.00	0.00	3.00
$5.0e-4$	433	-0.01	3.00	-0.01	3.00	0.00	3.00
$2.5e-4$	866	-0.01	3.00	-0.01	3.00	0.00	3.00
$1.0e-4$	2165	-0.01	5.19	-0.01	3.00	0.00	3.00
$5.0e-5$	4330	-6.72	169.93	-0.01	3.08	0.00	3.00
$2.5e-5$	8660	$-4.8e+6$	$1.3e+7$	-0.01	14.72	0.00	3.00
$1.0e-5$	21651			$-7.3e+3$	$3.1e+4$	0.00	26.11
$5.0e-6$	43301					-14.89	36.25

In Table 3, the numbers of GMRES iterations are given without preconditioning. The GMRES solver for the proposed BEM-based FEM converges faster than for the preceding scheme. For increasing ℓ the convergence slightly improves. Furthermore, the iteration numbers stay bounded without the help of any preconditioning until the maximum principle is violated.

5.2.2 Experiment 2

In the next numerical experiment, we consider a convection-diffusion problem with non-constant convection vector. In order to compare the experiments, let $\Omega = (0,1)^3$. We solve

$$\begin{aligned} -\alpha\Delta u + b \cdot \nabla u &= 0 \quad \text{in } \Omega, \\ u &= g \quad \text{on } \Gamma, \end{aligned}$$

Table 3: Comparing GMRES-iterations in Experiment 1 for the straightforward method and $\ell = 1, 2, 3$.

α	s.f.	$\ell = 1$	$\ell = 2$	$\ell = 3$
$5.0e-3$	30	28	25	23
$2.5e-3$	33	28	26	24
$1.0e-3$	36	28	26	24
$5.0e-4$	36	28	25	23
$2.5e-4$	311	28	24	23
$1.0e-4$	300	30	24	23
$5.0e-5$		49	25	23
$2.5e-5$		302	31	23
$1.0e-5$			92	29
$5.0e-6$				55

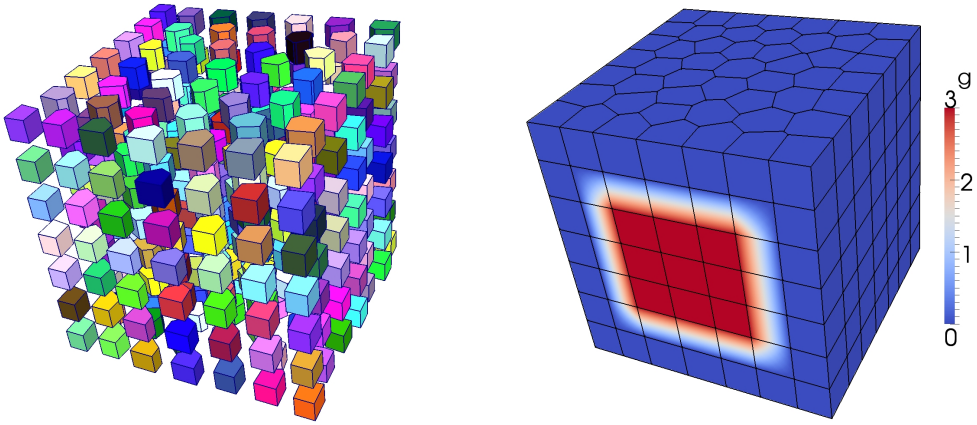

Figure 3: Visualisation of polyhedral mesh and Dirichlet data for Experiment 2.

where

$$b(x) = \frac{0.85}{\sqrt{(1-x_1)^2 + (1-x_3)^2}} \begin{pmatrix} x_3 - 1 \\ 0 \\ 1 - x_1 \end{pmatrix}$$

and g is chosen such that it is piecewise bilinear and continuous with $0 \leq g \leq 3$ on one side of the unit cube and zero on all others, see Figure 3. The convection vector b is scaled in such a way that the Péclet numbers in the computations are comparable with those of Experiment 1. The convection is a rotating field around the upper edge of the unit cube Ω, which lies in the front when looking at Figure 3. Consequently, we expect that the non-zero Dirichlet data is transported towards the upper side of the cube for low diffusion.

This time, the domain Ω is decomposed into prisms having general polygonal ends, see Figure 3. The polyhedral mesh consists of 350 elements, 1450 faces, 1907 edges and 808 nodes of which 438 nodes lie in the interior of Ω. Thus, the number of degrees of freedom in the BEM-based FEM is equal to 438. The maximal diameter of the elements is $h_{\max} \approx 0.25$ and the discretization was chosen such that $h_{\max}$ is approximately the same as in Experiment 1.

In our experiments, the polyhedral mesh has less elements, faces and edges than the tetrahedral discretization. This is beneficial concerning the computations in the preprocessing step. Less local problems have to be solved on edges and faces and there are less boundary element matrices which have to be set up. Furthermore, polyhedral discretizations admit a high flexibility while meshing complex geometries.

In Table 4, we list the minimal and maximal values of the approximation u_ℓ on the skeleton for $\ell = 2$ to verify the discrete maximum principle. Furthermore, the numbers of GMRES iterations are given with and without preconditioning.

The first observation is that the number of GMRES iterations increases when the diffusion α tends to zero. Thus, the iteration count is not bounded in this experiment. However, this behavior correlates with the violation of the maximum principle and is therefore the result of inaccuracies. Already with the help of the simple geometric row scaling preconditioner, we overcome the increase of the iteration number.

A more detailed discussion is needed for the discrete maximum principle. In Table 4, we observe that this principle is violated in a relatively early stage for $\alpha = 2.5e-2$,

Table 4: Verifying maximum principle in Experiment 2 for $\ell = 2$ and number of iterations with/without preconditioning.

α	Pe_h	$u_{\min}$	$u_{\max}$	iter.	iter. (prec.)
$1.0e-1$	2	0.00	3.00	20	20
$5.0e-2$	4	0.00	3.00	20	21
$2.5e-2$	9	0.00	3.04	20	21
$1.0e-2$	22	0.00	3.07	23	22
$5.0e-3$	43	-0.01	3.26	29	23
$2.5e-3$	86	-0.04	3.37	42	24
$1.0e-3$	216	-0.10	3.38	45	23
$5.0e-4$	431	-0.13	3.45	48	22
$2.5e-4$	863	-0.15	3.51	51	21
$1.0e-4$	2157	-0.15	3.53	52	21
$5.0e-5$	4313	-0.16	3.57	58	23
$2.5e-5$	8627	-0.25	4.38	69	28

which corresponds to $\mathrm{Pe}_h = 9$. However, the increase of $u_{\max}$ and the decrease of $u_{\min}$ is fairly slow for increasing Péclet number.

Here, one has to point out that the computations are done on a polyhedral mesh with a globally continuous approximation u_ℓ. This, by itself, is a current field of research even without dominant convection, see [1]. The geometry of polygonal faces is more complex than the triangles in Experiment 1, and thus, the computations on the faces are more involved.

Figure 4 shows the approximation of two different basis functions over the same polygonal face, the auxiliary triangulation and the projected convection vector. We can see how the local mesh has been adapted to the underlying differential operator, namely by moving the node, which lay initially in the center of the polygon, into the direction of the convection. In certain constellations, the boundary layers are not resolved appropriately. In the left picture of Figure 4, the approximation of the basis function is satisfactory. In the right picture, however, oscillations occur in the lower right corner due to the relatively large triangles near the boundary. In many cases these situations are already resolved quite well by the simple mesh adaptation. When we introduced the moving of the auxiliary nodes in the implementation, the numerical results improved. Thus, we expect that a better adaptation of the local meshes, and consequently a better approximation of the local problems, improves the stability of the BEM-based FEM such that we would obtain comparable results to Experiment 1 for the discrete maximum principle.

Finally, in Figure 5, the approximation u_ℓ is visualized for $\ell = 2$ and two different values of diffusion $\alpha = 2.5e-2$ and $\alpha = 5.0e-5$. The domain Ω has been cut through, such that the approximation is visible on a set of polygonal faces which lie in the interior of the domain. The expected behavior of the solution can be observed. The Dirichlet data is transported into the interior of the domain along the convection vector. In the case of the convection-dominated problem, oscillations appear near the outflow boundary.

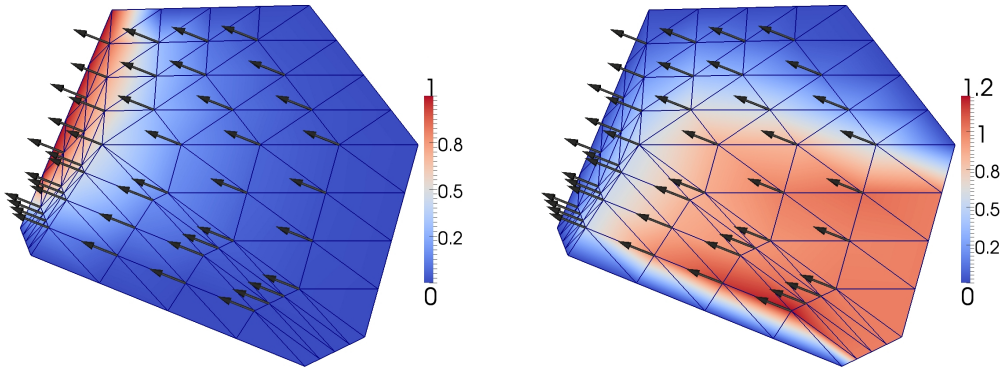

Figure 4: Approximations of basis functions on polygonal face, projected convection vector and auxiliary triangulation with appropriately (left) and not appropriately (right) resolved boundary layer.

6 Conclusion

We have derived new convection-adapted BEM-based FEM discretization schemes for convection-diffusion-reaction boundary value problems that considerably extend the range of applicability with respect to the strength of convection. The numerical results have not only confirmed this enhanced stability property of the discretization scheme, but have also indicated faster convergence of the GMRES solver in comparison with the original BEM-based FEM scheme presented in [16, 14].

References

[1] L. Beirão da Veiga, F. Brezzi, L. .D. Marini, and A. Russo. Virtual element methods for general second order elliptic problems on polygonal meshes. *ArXiv e-prints, arXiv:1412.2646*, 2014.

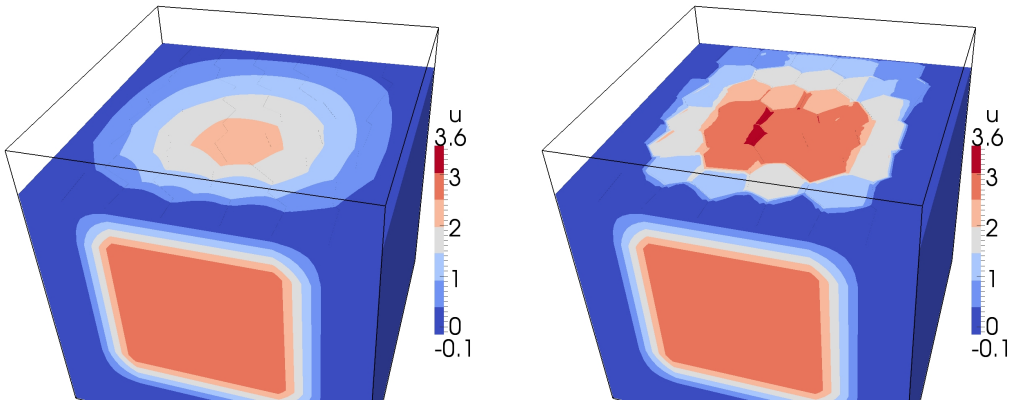

Figure 5: Cut through the domain $\Omega = (0, 3)^3$ and visualisation of the approximation in Experiment 2 for $\alpha = 2.5e - 2$ (left) and $\alpha = 5.0e - 5$ (right).

[2] F. Brezzi, M.-O. Bristeau, L. P. Franca, M. Mallet, and G. Rogé. A relationship between stabilized finite element methods and the Galerkin method with bubble functions. *Comput. Meth. Appl. Mech. Engrg.*, 96(1):117–129, 1992.

[3] F. Brezzi, L. P. Franca, T. J. R. Hughes, and A. Russo. $b = \int g$. *Comput. Meth. Appl. Mech. Engrg.*, 145(3–4):329–339, 1997.

[4] F. Brezzi, T. J. R. Hughes, L. D. Marini, A. Russo, and E. Süli. A priori error analysis of residual-free bubbles for advection-diffusion problems. *SIAM J. Numer. Anal*, 36(6):1933–1948, 1999.

[5] F. Brezzi, D. Marini, and A. Russo. Applications of the pseudo residual-free bubbles to the stabilization of convection-diffusion problems. *Comput. Meth. Appl. Mech. Engrg.*, 166(1–2):51–63, 1998.

[6] A. N. Brooks and T. J. R. Hughes. Streamline upwind/Petrov-Galerkin formulations for convection dominated flows with particular emphasis on the incompressible Navier-Stokes equations. *Comput. Method. Appl. M.*, 32(1-3):199 – 259, 1982.

[7] D. Copeland, U. Langer, and D. Pusch. From the boundary element domain decomposition methods to local Trefftz finite element methods on polyhedral meshes. In M. Bercovier, M. Gander, R. Kornhuber, and O. Widlund, editors, *Domain decomposition methods in science and engineering XVIII*, volume 70 of *Lect. Notes Comput. Sci. Eng.*, pages 315–322. Springer, Berlin Heidelberg, 2009.

[8] M. Costabel. Symmetric methods for the coupling of finite elements and boundary elements. In C.A. Brebbia, W.L. Wendland, and G. Kuhn, editors, *Boundary Elements IX*, pages 411–420. Springer, Berlin, Heidelberg, New York, 1987.

[9] Y. Efendiev, J. Galvis, R. Lazarov, and S. Weißer. Mixed FEM for second order elliptic problems on polygonal meshes with BEM-based spaces. In I. Lirkov, S. Margenov, and J. Waśniewski, editors, *Large-Scale Scientific Computing*, Lect. Notes Comput. Sc., pages 331–338. Springer, Berlin Heidelberg, 2014.

[10] L. P. Franca, A. Nesliturk, and M. Stynes. On the stability of residual-free bubbles for convection-diffusion problems and their approximation by a two-level finite element method. *Comput. Meth. Appl. Mech. Engrg.*, 166(1–2):35–49, 1998.

[11] V. Girault and P.-A. Raviart. *Finite element methods for Navier-Stokes equations*, volume 5 of *Springer Series in Computational Mathematics*. Springer-Verlag, Berlin, 1986.

[12] D. Gordon and R. Gordon. Row scaling as a preconditioner for some nonsymmetric linear systems with discontinuous coefficients. *J. Comput. Appl. Math.*, 234(12):3480–3495, 2010.

[13] C. Hofreither. L_2 error estimates for a nonstandard finite element method on polyhedral meshes. *J. Numer. Math.*, 19(1):27–39, 2011.

[14] C. Hofreither. *A Non-standard Finite Element Method using Boundary Integral Operators*. PhD thesis, Johannes Kepler University, Linz, Austria, December 2012.

[15] C. Hofreither, U. Langer, and C. Pechstein. Analysis of a non-standard finite element method based on boundary integral operators. *Electron. Trans. Numer. Anal.*, 37:413–436, 2010.

[16] C. Hofreither, U. Langer, and C. Pechstein. A non-standard finite element method for convection-diffusion-reaction problems on polyhedral meshes. *AIP Conference Proceedings*, 1404(1):397–404, 2011.

[17] C. Hofreither, U. Langer, and C. Pechstein. FETI solvers for non-standard finite element equations based on boundary integral operators. In J. Erhel, M.J. Gander, L. Halpern, G. Pichot, T. Sassi, and O.B. Widlund, editors, *Domain Decomposition Methods in Science and Engineering XXI*, volume 98 of *Lect. Notes Comput. Sci. Eng.*, pages 731–738. Springer, Heidelberg, 2014.

[18] G. C. Hsiao, O. Steinbach, and W. L. Wendland. Domain decomposition methods via boundary integral equations. *J. Comput. Appl. Math.*, 125(1–2):521–537, 2000.

[19] G. C. Hsiao and W. L. Wendland. Domain decomposition in boundary element methods. In R. Glowinski, Y. A. Kuznetsov, G. Meurant, J. Périaux, and O. B. Widlund, editors, *Proceedings of the Fourth International Symposium on Domain Decomposition Methods for Partial Differential Equations, Moscow, May 21–25, 1990*, pages 41–49. SIAM, Philadelphia, 1991.

[20] G. C. Hsiao and W. L. Wendland. *Boundary Integral Equations*. Springer, Heidelberg, 2008.

[21] N. Kopteva and E. O'Riordan. Shishkin meshes in the numerical solution of singularly perturbed differential equations. *Int. J. Numer. Anal. Mod.*, 7(3):393–415, 2010.

[22] T. Linß. *Layer-adapted meshes for reaction-convection-diffusion problem*, volume 1985 of *Lecture Notes in Mathematics*. Springer-Verlag, Berlin, 2010.

[23] W. McLean. *Strongly Elliptic Systems and Boundary Integral Equations*. Cambridge University Press, Cambridge, UK, 2000.

[24] S. Rjasanow and S. Weißer. Higher order BEM-based FEM on polygonal meshes. *SIAM J. Numer. Anal.*, 50(5):2357–2378, 2012.

[25] S. Rjasanow and S. Weißer. FEM with Trefftz trial functions on polyhedral elements. *J. Comput. Appl. Math.* , 263:202–217, 2014.

[26] H.-G. Roos, M. Stynes, and L. Tobiska. *Robust numerical methods for singularly perturbed differential equations*, volume 24 of *Springer Series in Computational Mathematics*. Springer–Verlag, Berlin, second edition, 2008.

[27] Y. Saad and M. H. Schultz. GMRES: a generalized minimal residual algorithm for solving nonsymmetric linear systems. *SIAM J. Sci. Statist. Comput.*, 7(3):856–869, 1986.

[28] S. A. Sauter and C. Schwab. *Boundary Element Methods*, volume 39 of *Springer Series in Computational Mathematics*. Springer, Berlin, Heidelberg, 2011.

[29] G. I. Shishkin. A difference scheme for a singularly perturbed equation of parabolic type with a discontinuous initial condition. *Dokl. Akad. Nauk SSSR*, 300(5):1066–1070, 1988.

[30] O. Steinbach. *Numerical Approximation Methods for Elliptic Boundary Value Problems. Finite and Boundary Elements*. Springer-Verlag, New York, 2008.

[31] S. Weißer. Residual error estimate for BEM-based FEM on polygonal meshes. *Numer. Math.*, 118(4):765–788, 2011.

[32] S. Weißer. *Finite Element Methods with local Trefftz trial functions*. PhD thesis, Universität des Saarlandes, Saarbrücken, Germany, September 2012.

[33] S. Weißer. Arbitrary order Trefftz-like basis functions on polygonal meshes and realization in BEM-based FEM. *Comput. Math. Appl.*, 67(7):1390–1406, 2014.

[34] S. Weißer. BEM-based finite element method with prospects to time dependent problems. In E. Oñate, J. Oliver, and A. Huerta, editors, *Proceedings of the jointly organized WCCM XI, ECCM V, ECFD VI, Barcelona, Spain, July 2014*, pages 4420–4427. International Center for Numerical Methods in Engineeering (CIMNE), 2014.

[35] S. Weißer. Higher order Trefftz-like Finite Element Method on meshes with L-shaped elements. In G. Leugering P. Steinmann, editor, *Special Issue: 85th Annual Meeting of the International Association of Applied Mathematics and Mechanics (GAMM), Erlangen 2014*, volume 14 of *PAMM*, pages 31–34. WILEY-VCH Verlag, 2014.

[36] S. Weißer. Residual Based Error Estimate for Higher Order Trefftz-Like Trial Functions on Adaptively Refined Polygonal Meshes. In A. Abdulle, S. Deparis, D. Kressner, F. Nobile, and M. Picasso, editors, *Numerical Mathematics and Advanced Applications - ENUMATH 2013*, volume 103 of *Lect. Notes Comput. Sci. Eng.*, pages 233–241. Springer International Publishing, 2015.